IEEE Access
Multidisciplinary | Rapid Review | Open Access Journal

Received March 26, 2019, accepted April 11, 2019, date of publication April 15, 2019, date of current version April 29, 2019.

Digital Object Identifier 10.1109/ACCESS.2019.2911400

A Novel Composite Control Algorithm for Restraining Nonlinear Superfluous Forces

LINGXIAO QUAN[1,2], YAOYAO MIAO[1], CHANGHONG GUO[1], AND QIN ZHANG[3]

[1]School of Mechanical Engineering, Yanshan University, Qinhuangdao 066004, China
[2]Hebei Heavy Machinery Fluid Power Transmission and Control Laboratory, Yanshan University, Qinhuangdao 066004, China
[3]Biological Systems Engineering, Washington State University, Pullman, WA 61801, USA

Corresponding author: Lingxiao Quan (lingxiao@ysu.edu.cn)

This work was supported by the National Natural Science Foundation of China under Grant 51775477 and Grant 51505410.

ABSTRACT A novel composite control algorithm is proposed to restrain nonlinear superfluous forces of a dual-channel load simulator. The dual-channel load simulator is utilized to measure the dynamic characteristic of an integrated hydraulic driving unit. The superfluous force cannot be avoided almost certainly and show a strong nonlinearity. Based on the speed synchronizing control algorithm, the composite control algorithm considers the two non-linear time-varying parameters of the flow gain *Kq* and the flow pressure gain *Kc* of the servo valve, and further considers the non-linearity and time-varying of the position disturbance electro-hydraulic servo control system. The fuzzy self-tuning PID control is applied to automatically adjust the PID parameters so that the superfluous force of the system can achieve the desired control effect. The accurate simulation of the load force is realized.

INDEX TERMS Nonlinear superfluous forces control, parameter self-tuning control algorithm, speed synchronizing control algorithm.

I. INTRODUCTION

The dynamic characteristic of the actuator is critical for the control effect of all hydraulic control system. It could play a decisive role for the high performance equipment, e.g., hydraulic robotics, wind turbines, cold rolling and aircraft. The hydraulic driving unit (HDU) which is composed with a servo valve and a cylinder is a common and indispensable hydraulic device of the hydraulic control system of the hydraulic quadruped robot (HQR) [1]. Many academics have performed considerable researches on the control algorithm of the HDU [2], [3]. It is especially important to use a novel and intelligent control algorithm to overcome the impact of various nonlinear, time-varying factors [4]–[6]. The dual-channel load simulator (DCLS) which is composed of a bearing channel and a loading channel is very important and frequent in control research [7]. Many control algorithms are tested by the DCLS. However, the superfluous force of the DCLS is an inevitable obstacle to carry out those control algorithm testing [8]. The structural compensation and the control algorithm are all common methods to restrain the superfluous forces [9]. The structure compensation method is simple and convenient, which needs to increase the necessary mechanical equipment or hydraulic components, such as double valve flow compensation [10]–[12]. However, the control algorithm is simple and feasible, and has a good economy [13].Besides, it is also effective in improving the robustness of the channel and reducing the mutual interference between the two channels [14].

Recently, much of the research has concentrated on the unknown model parameters of the DCLS and the uncertain external disturbance of the force control channel (FCC). These research results have proved that the effect of the nonlinear outside interference could be effectively reduced, and the robustness of the channels could be improved if the control algorithms are adopted. A lot of researches have been conducted on restraining the surplus force of load simulator by robust control, such as mu theory [15], Quantitative feedback theory (QFT) [16], [17], pre and feedback robust control method, H∞ robust control [18] and so on. Yuan designed a robust controller based on the composite sensitivity H∞ to decrease the superfluous torque caused by various uncertain parameters and force distance in the electro-hydraulic load simulator [19]. Skupin proposed adaptive feed forward decoupling controller for MIMO nonlinear hydraulic system, and incorporated it into PLC controller to improve

The associate editor coordinating the review of this manuscript and approving it for publication was Tao Wang.

the dynamic control effect of load simulation system [20]. Wang proposed a hybrid control strategy of feed forward fuzzy adaptive PID control, which improves the tracking precision of force control [21]. Ahn presented an online self-tuning fuzzy PID controller to improve the control performance of a loading system and to eliminate or reduce the disturbance [22]. Truong, et al. suggested a grey prediction model combined with a fuzzy PID controller to improve the control quality of the loading system while eliminating or reducing the disturbance. Furthermore, fuzzy controllers and a tuning algorithm are used to change the grey step size in order to improve the control quality by them [23].

In addition, previous studies state that it was beneficial to decrease the mutual interference between two channels with an intelligent control algorithm. Jiao improved the traditional speed synchronizing control algorithm (SSCA) to remove the superfluous force of the electric-hydraulic simulator [24], [25]. Jacazio proposed an optimal equalization control strategy to minimize the opposing forces between two redundant electro-hydraulic servo-actuators connected to the same flight control surface [26]. Zhou provided one new structure invariance principle with the particle swarm optimization algorithm to identify parameters of the system, and established the mathematical model to improve the effect of restraining superfluous [27].

From our perspectives, although huge gains have been realized by these methodologies, they should be increasingly employed to create a control algorithm in order to improve the robustness of the channel deeply, at the same time the mutual interference between the two channels decreased.

In this study, a novel composite control algorithm (CCA) has been proposed to restrain nonlinear superfluous forces of the DCLS. Through the comparison of control effect between CCA and SSCA and parameter self-tuning control algorithm (PSCA), it indicates that CCA could achieve strong robustness and ability to overcome the impact of nonlinear factors.

This paper is organized as follows. Section II introduces the working principle, the mathematical model and the control block diagram of the DCLS. Section III illustrates the mathematical model of the three control algorithms and compares their strengths and weaknesses. Section IV compares the restraining effect of the three control algorithms with different force loads and position interferences. Finally, Section V presents the conclusions.

II. MATHEMATICAL MODEL OF THE TEST PLATFORM

DCLS is used to test the response performance of hydraulic quadruped robot's HDU under no-load and complex load spectrum, and is used to verify the control effect of HDU control strategy in actual operation. The DCLS is shown in Fig. 1. The DCLS is composed of two identical HDU. The right HDU is the bearing channel with a position closed loop. It is considered to be the position control channel (PCC), and is used to simulate the leg motion of the HQR. The left HDU is the loading channel with a closed-loop force. It is considered to be the FCC, and is used to simulate the loading force received by the leg joints of the HQR. The two hydraulic cylinders are installed on one rigidly steel support. They are connected with one junction at each other, and one high precision force sensor is placed at the junction.

In order to facilitate the derivation of the equation, the following assumptions are made:

(1)The slide valve is a kind of ideal zero opening four side slide valves. The four throttle windows are matched and symmetrical.

(2)The flow of the throttle window is turbulent. The effect of oil compressibility could be not considered.

(3)The hydraulic cylinder is an ideal symmetrical cylinder. The pressure of each point in each work cavity is the same ones with neglecting the influence of oil temperature.

(4)The oil supply pressure is constant, and the oil back pressure is zero.

(5)The pressure loss, the fluid quality influence and the dynamic influence of the internal piping of the servo cylinder could be negligible.

Based on the above assumptions, there are three basic equations.

$$Q = K_q x_v - K_c p \tag{1}$$

$$Q = A\frac{dx}{dt} + C_{tp}p + \frac{V_t}{4\beta_e}\frac{dp}{dt} \tag{2}$$

$$Ap = m\frac{d^2x}{dt^2} + B_p\frac{dx}{dt} + Kx + F \tag{3}$$

where Q is system flow, K_q is servo valve flow gain, K_c is servo valve flow pressure gain, x_v is spool displacement, p is load pressure, A is hydraulic cylinder piston area, x is hydraulic cylinder piston displacement, C_{tp} is the total leakage coefficient of the hydraulic cylinder, V_t is the total compression volume of the hydraulic cylinder, β_e is the effective bulk modulus of elasticity, B_p is the viscous damping coefficient of the piston and load, K is the load spring stiffness, m is piston and load conversion to the general quality of the piston, F is load acting on the piston external force.

The cylinder tube and the piston could be designed and installed with minimal clearance. The cavity of the cylinder is small. The stiffness of the cylinder and the support is strong. Therefore, we assume that the friction and internal leakage of the cylinder, Viscous damping of the cylinder, the fluid compression and the load stiffness could be ignored. According to these assumptions, the three simplified equations of the valve-controlled cylinder are given as follows

$$Q = K_q x_v - K_c p \tag{4}$$

$$Q = A\frac{dx}{dt} \tag{5}$$

$$Ap = m\frac{d^2x}{dt^2} + F \tag{6}$$

After applying a Laplace transform and simplifying the results, the open-loop transfer functions of the PCC and the

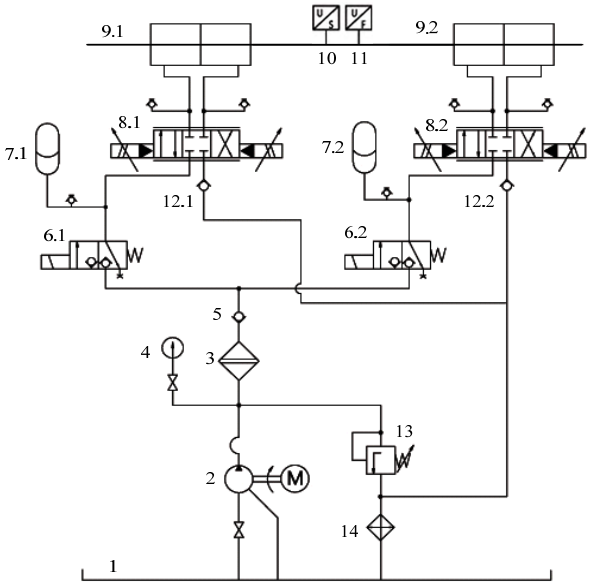

(a)

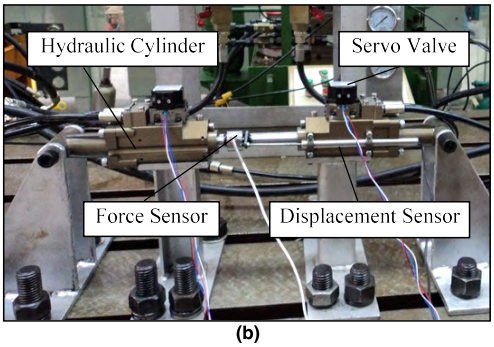

(b)

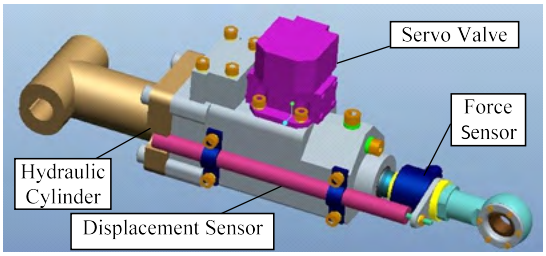

(C)

FIGURE 1. The schematic diagram of the hydraulic system of the DCLS. (a) The schematic diagram of the hydraulic system of the DCLS. 1. Tank 2. Hydraulic pump 3. Filter 4. Pressure gauge 5. Unidirectional valve 6. Commutation Valve. 7. Accumulator. 8. Servo valve. 9. Hydraulic cylinder. 10. Displacement sensor. 11. Force sensor. 12. Unidirectional valve. 13. Relief valve. 14. Cooler. (b) Test bench for DCLS. (c) 3d assembly model of the HDU.

FCC are (7) and (8).

$$X_{\mathrm{w}} = \left(\frac{A_{\mathrm{w}}K_{\mathrm{qw}}}{K_{\mathrm{cw}}}X_{\mathrm{vw}} - F_{\mathrm{w}}\right) \Bigg/ \left[\left(m_{\mathrm{w}}s + \frac{A_{\mathrm{w}}^2}{K_{\mathrm{cw}}}\right)s\right] \tag{7}$$

$$F_{\mathrm{L}} = \frac{A_{\mathrm{L}}K_{\mathrm{qL}}}{K_{\mathrm{cL}}}X_{\mathrm{vL}} - \left(m_{\mathrm{L}}s + \frac{A_{\mathrm{L}}^2}{K_{\mathrm{cL}}}\right)sX_{\mathrm{L}} \tag{8}$$

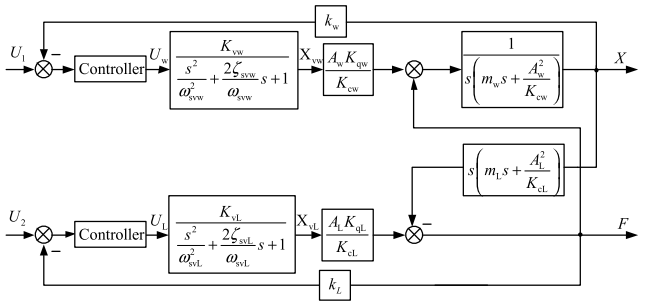

FIGURE 2. Block diagram of the mathematical model of the test platform.

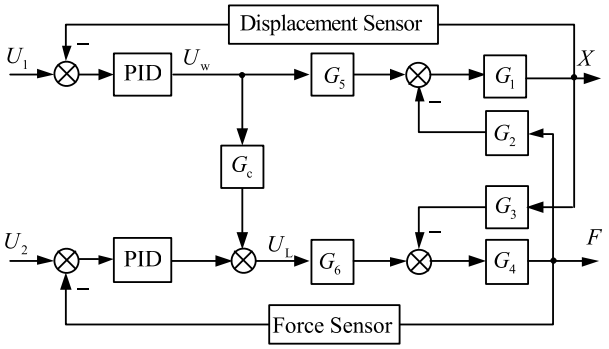

FIGURE 3. Schematic diagram of the speed synchronization control.

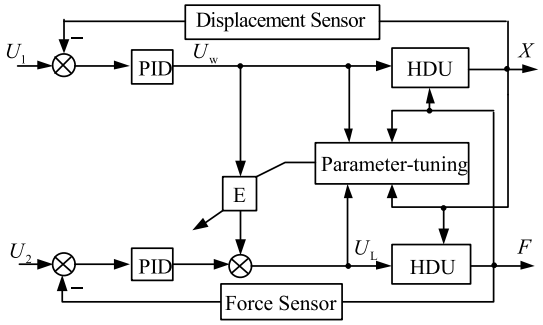

FIGURE 4. Schematic diagram of the PSCA.

Considering the servo valve as a second-order oscillator, the transfer function is described as

$$\frac{X_{\mathrm{v}}}{U} = \frac{K_{\mathrm{v}}}{\frac{s^2}{\omega_{\mathrm{sv}}^2} + \frac{2\zeta_{\mathrm{sv}}}{\omega_{\mathrm{sv}}}s + 1} \tag{9}$$

where U is servo valve amplifier input voltage, K_{v} is servo valve voltage spool displacement gain, ω_{sv} is servo valve natural frequency, ζ_{sv} is servo valve with damping ratio.

Because the response frequency of the displacement sensor is much higher than that hydraulic system, it could be regarded as a proportional link, for which its transfer function is as follows

$$k_{\mathrm{w}} = \frac{U_{\mathrm{gw}}}{X} \tag{10}$$

where k_{w} is the gain of the displacement sensor, U_{gw} is the output voltage of the displacement sensor.

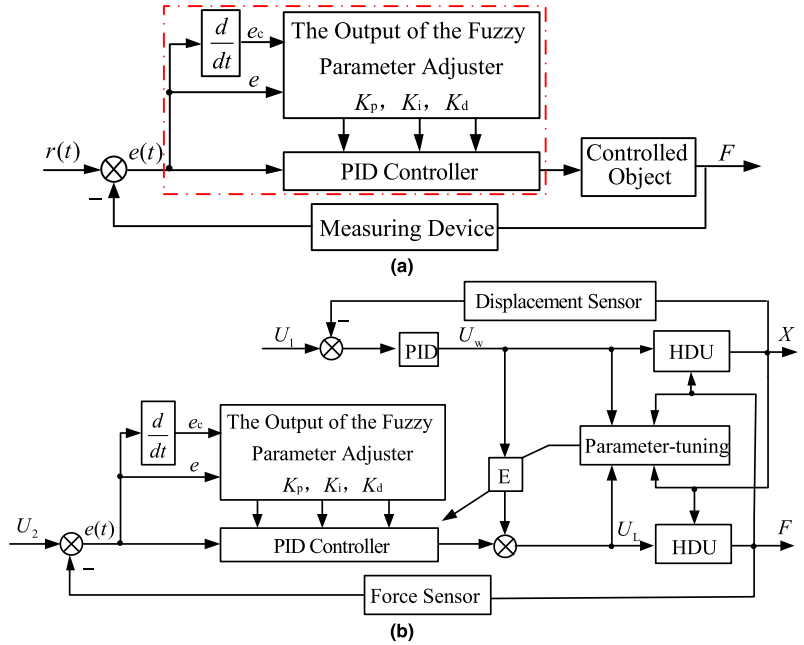

FIGURE 5. Composite control algorithm. (a) The structure principle of fuzzy self-tuning PID. (b) Schematic diagram of the CCA.

The force sensor also can be regarded as a proportion link, for which its transfer function is as follows

$$k_{\mathrm{L}} = \frac{U_{\mathrm{gL}}}{F} \tag{11}$$

where k_{L} is the gain of the force sensor, U_{gL} is the output voltage of the force sensor.

The relationship between the parameters of the two cylinders is $A_{\mathrm{w}} = A_{\mathrm{L}} = A$, $m_{\mathrm{w}} = m_{\mathrm{L}} = m$, $X_{\mathrm{w}} = X_{\mathrm{L}} = X$ and $F_{\mathrm{w}} = -F_{\mathrm{L}} = F$. By the (7)-(11), the control block diagram of the DCLS is shown in Fig. 2.

III. CONTROL ALGORITHM AND MODEL

A. MATHEMATICAL MODEL OF SPEED SYNCHRONIZING CONTROL ALGORITHM

The SSCA is a good way to restrain superfluous forces, and it is employed to eliminate the interference from the PCC to the FCC. One compensation link, G_{c}, is added and is used to construct the model of the SSCA as

$$G_{\mathrm{c}} \cdot G_6 = G_1 \cdot G_3 \cdot G_5 \tag{12}$$

Its control block diagram is shown in Fig. 3.

By comparing Fig. 4 with Fig. 5, $G_2 = -1$, $G_4 = 1$, the expressions for link G_1, G_3, G_5, and G_6 are obtained as the following equations

$$G_1 = \frac{1}{s\left(m_{\mathrm{w}} s + \frac{A_{\mathrm{w}}^2}{K_{\mathrm{cw}}}\right)} \tag{13}$$

$$G_3 = s\left(m_{\mathrm{L}} s + \frac{A_{\mathrm{L}}^2}{K_{\mathrm{cL}}}\right) \tag{14}$$

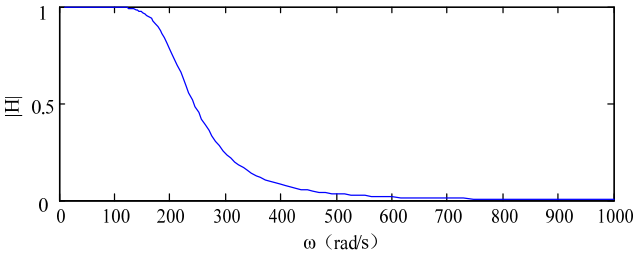

FIGURE 6. Amplitude frequency characteristic curve of Butterworth low pass filter.

$$G_5 = \frac{K_{\mathrm{vw}}}{\frac{s^2}{\omega_{\mathrm{svw}}^2} + \frac{2\zeta_{\mathrm{svw}}}{\omega_{\mathrm{svw}}} s + 1} \cdot \frac{A_{\mathrm{w}} K_{\mathrm{qw}}}{K_{\mathrm{cw}}} \tag{15}$$

$$G_6 = \frac{K_{\mathrm{vL}}}{\frac{s^2}{\omega_{\mathrm{svL}}^2} + \frac{2\zeta_{\mathrm{svL}}}{\omega_{\mathrm{svL}}} s + 1} \cdot \frac{A_{\mathrm{L}} K_{\mathrm{qL}}}{K_{\mathrm{cL}}} \tag{16}$$

The compensation link for the superfluous force is defined as E and could be derived as (17), when (13)-(16) are substituted into (12).

$$E = G_{\mathrm{c}} = \frac{A_{\mathrm{w}} K_{\mathrm{vw}} K_{\mathrm{qw}}}{A_{\mathrm{L}} K_{\mathrm{vL}} K_{\mathrm{qL}}} \cdot \left(\frac{K_{\mathrm{cL}} m_{\mathrm{L}} s + A_{\mathrm{L}}^2}{K_{\mathrm{cw}} m_{\mathrm{w}} s + A_{\mathrm{w}}^2}\right) \tag{17}$$

Because of the symmetry of the two channels, the differences in the flow gain and in the flow-pressure coefficient of the two servo valves could be ignored. Therefore, the relationships of K_{qw}, K_{qL}, K_{cw} and K_{cL}, are considered to be $K_{\mathrm{qw}} \approx K_{\mathrm{qL}}$ and $K_{\mathrm{cw}} \approx K_{\mathrm{cL}}$. Furthermore, it can be shown that $E = 1$.

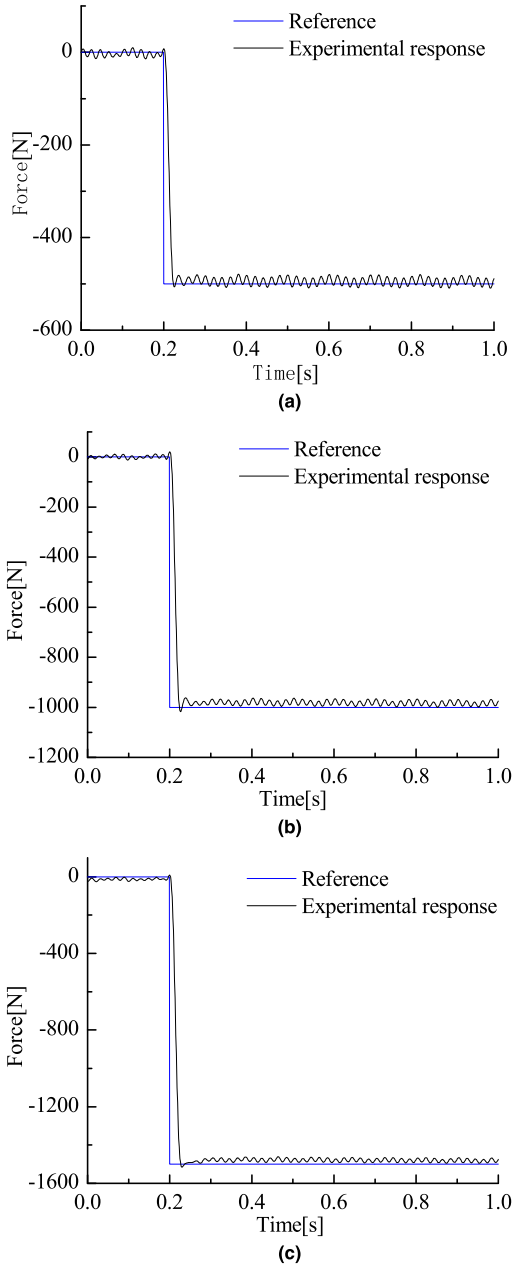

FIGURE 7. Step response curves of FCC. (a) Step response of FCC at $f_F = 500$ N. (b) Step response of FCC at $f_F = 1000$ N. (c) Step response of FCC at $f_F = 1500$ N.

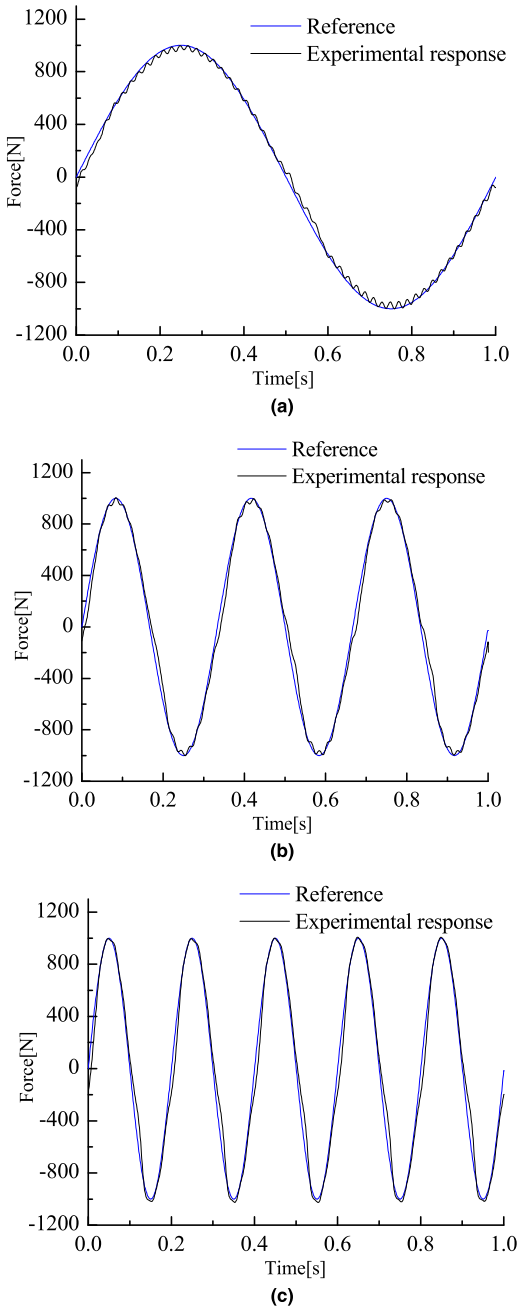

FIGURE 8. Sinusoidal response curves of FCC. (a) Sinusoidal response of FCC at $f_F = 1$ Hz. (b) Sinusoidal response of FCC at $f_F = 3$ Hz. (c) Sinusoidal response of FCC at $f_F = 5$ Hz.

It proves that the superfluous force cannot be ideally restrained by the SSCA because of the nonlinear factors, such as the flow-pressure nonlinearity of the servo valve. This conclusion has been verified with a simulation. The simulation results are in accordance with the traditional ones, and they are not presented in this paper.

B. MATHEMATICAL MODEL OF PARAMETER SELF-TUNING CONTROL ALGORITHM

SSCA could greatly restrain the superfluous force, but has not been fundamentally eliminated. The reasons are as follows

According to (17), the compensation link contains two time varying parameters, namely the servo valve flow gain K_q and the flow pressure gain K_c. They have great nonlinearity and time variation, and could vary with the working point and the external working condition of the valve. In the use of SSCA for restraining the superfluous force, without considering the nonlinear factors of the pressure flow of servo valve, only at a specific point, the superfluous force is restrained to achieve optimal effect. The other point is relatively poor, which may cause system oscillation and seriously affect the inhibitory effect of the superfluous force.

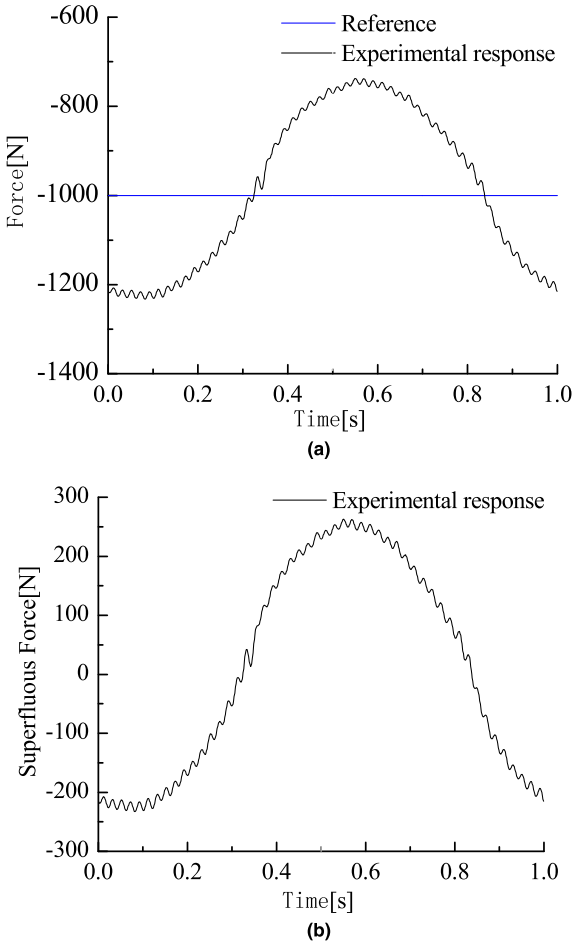

FIGURE 9. Response of FCC at $f_X = 1$Hz. (a) Experimental response curve. (b) Superfluous force curve.

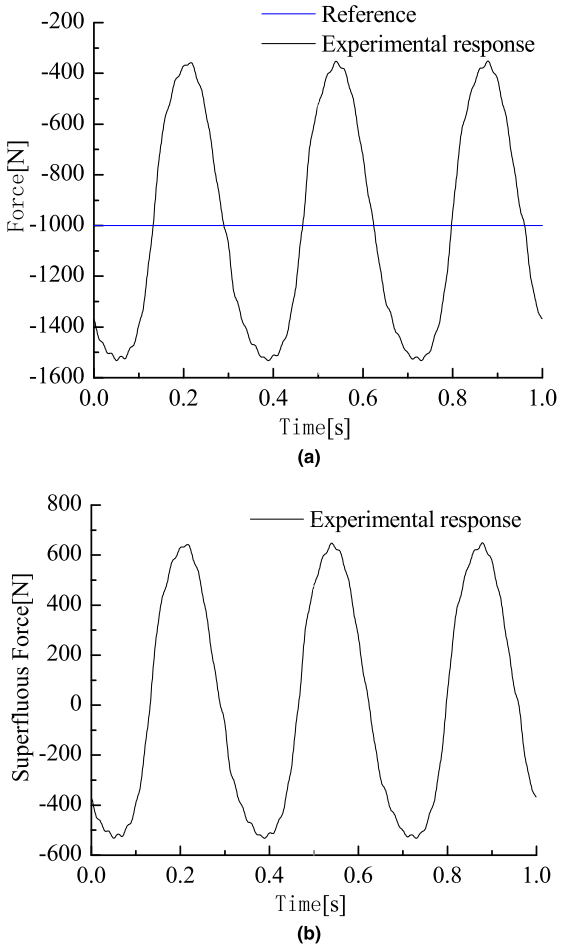

FIGURE 10. Response of FCC at $f_X = 3$Hz. (a) Experimental response curve. (b) Superfluous force curve.

In order to better restrain the superfluous force, the pressure flow nonlinear factor of the two system servo valves is considered, and the PSCA is further applied. By modifying the flow gain K_q and the flow pressure gain K_c online, the parameters of the compensator could be adjusted online, so that the compensator is always working near the best working point to improve the restraining effect of the superfluous force.

Note that (18)-(21) are commonly used [28]. If the letter w is added to the subscripts of K_q, K_c, K_u, K_v, C_v, W, x_v and P, these parameters are suitable for the servo valve of the PCC. Similarly, if the letter L is added to the subscripts of the above parameters, they are suitable for the servo valve of the FCC.

Equation (18) and (19) represent the flow gain K_q and the flow-pressure gain K_c of the servo valve, respectively. There is a nonlinear relationship between x_v and P_s.

$$K_q = C_v W \sqrt{\frac{1}{\rho}\left(P_s - sgn\left(x_v\right) P\right)} \tag{18}$$

$$K_c = \frac{1}{2} C_v W \left|x_v\right| \sqrt{\frac{1}{\rho\left(P_s - sgn\left(x_v\right) P\right)}} \tag{19}$$

where C_v is servo valve orifice flow coefficient, W is servo valve orifice area gradient, ρ is oil density, P_s is oil pressure.

The relationship between K_u and K_q is obtained as the following

$$K_u = K_v K_q \tag{20}$$

where K_u is voltage gain of servo valve flow. Combining (18) with (20), the function is obtained as

$$K_u = K_v C_v W \sqrt{\frac{1}{\rho}\left(P_s - sgn\left(U\right) P\right)} \tag{21}$$

The nonlinear factor of servo valve pressure flow is mainly considered. The difference in the two order vibration of the servo valve is ignored. Then the compensation link expression E can be simplified as.

$$E = \frac{K_{qw} K_{vw} (K_{cL} ms + A^2)}{K_{qL} K_{vw} (K_{cw} ms + A^2)} \tag{22}$$

Then, from (18)-(22), the PSCA model is given as (23), as shown at the bottom of the next page, where the parameter values of the two servo valves are approximately $C_{vw} = C_{vL} = 0.67$, $W_w = W_L = 1.256 \times 10^{-4}$, $K_{vw} = K_{vL} = 2 \times 10^{-4}$. Because of the relationship between F_L, F_w and

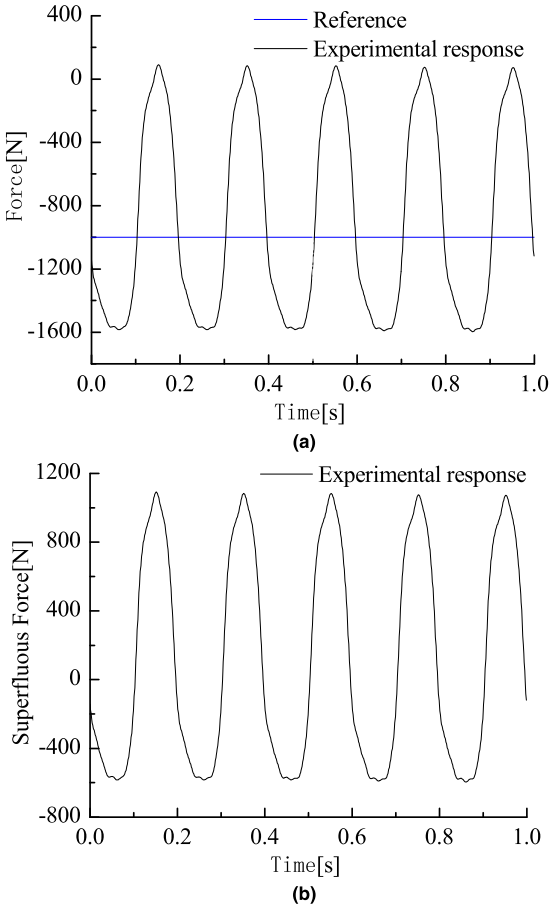

FIGURE 11. Response of FCC at $f_X = 5$Hz. (a) Experimental response curve. (b) Superfluous force curve.

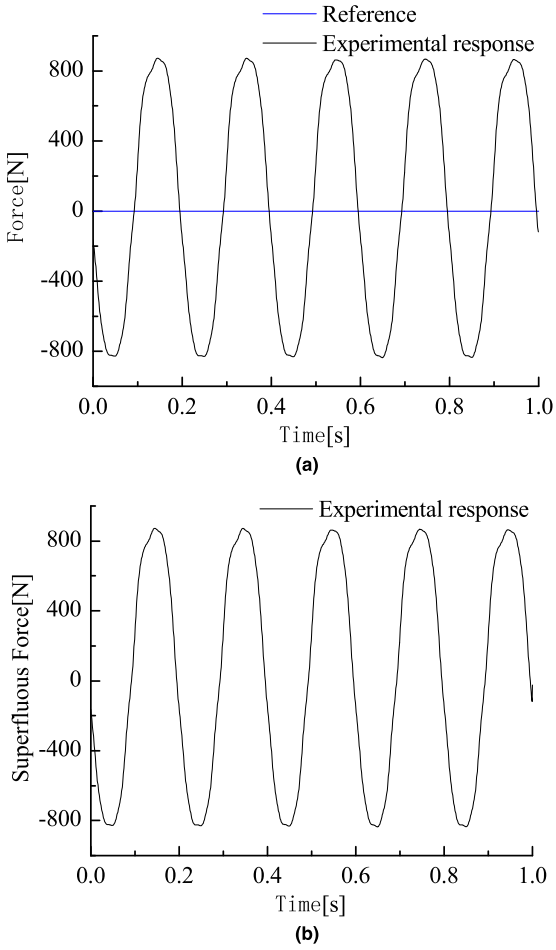

FIGURE 12. Response of FCC at $f_F = 0$ N. (a) Experimental response curve. (b) Superfluous force curve.

F is F_{L} =-F_{w} = F, the pressure functions of the two cylinders are $P_{\mathrm{w}} = \left(ms^2X - F\right)/A$, $P_{\mathrm{L}} = \left(ms^2X + F\right)/A$.

The compensation link has a relationship with oil pressure, with the input voltage of the servo valve amplifier, with the output acceleration of the PCC and with the output force of the FCC. All of these relationships are nonlinear functions. Therefore, the compensation link has time-varying and dynamic nonlinear characteristics. To improve the restraining effect, the PSCA could adjust its parameters online by detecting the above variables in real-time.

The schematic diagram of the PSCA is shown in Fig. 4.

C. MATHEMATICAL MODEL OF COMPOSITE CONTROL ALGORITH

There are two methods to restrain the superfluous force and improve the accuracy of FCC. One is to reduce the impact of PCC on the FCC, the other is to improve the anti-interference ability of FCC itself. SSCA and PSCA only meet the first method. In order to improve the ability of dry anti-jamming of FCC, the CCA is proposed. The schematic diagram of the CCA is shown in Fig. 5. CCA is based on PSCA, adding fuzzy PID control to the forward channel of the FCC, adjusting the parameters of PID controller online, improving the anti-interference ability of the FCC, and further restraining the superfluous force.

Conventional PID controller is easy to apply, but the fixed PID parameters cannot adapt to the control system with changing parameter and more interference. Even when the parameter range is too large, the system performance could get worse obviously. Fuzzy control has a strong anti-jamming capability and can meet the requirements of control precision. We combined the PID control and fuzzy control to form a fuzzy PID control so as to gain a better control effect.

$$E = \frac{K_{\mathrm{uw}}\left(K_{\mathrm{cL}}ms + A^2\right)}{K_{\mathrm{uL}}\left(K_{\mathrm{cw}}ms + A^2\right)} = \frac{K_{\mathrm{vw}}C_{\mathrm{vw}}W_{\mathrm{w}}\sqrt{\frac{1}{\rho}\left(P_{\mathrm{s}} - sgn\left(U_{\mathrm{w}}\right)P_{\mathrm{w}}\right)}}{K_{\mathrm{vL}}C_{\mathrm{vL}}W_{\mathrm{L}}\sqrt{\frac{1}{\rho}\left(P_{\mathrm{s}} - sgn\left(U_{\mathrm{L}}\right)P_{\mathrm{L}}\right)}} \cdot \frac{\frac{1}{2}C_{\mathrm{vL}}W_{\mathrm{L}}\left|X_{\mathrm{vL}}\right|\sqrt{\frac{1}{\rho(P_{\mathrm{s}} - sgn(X_{\mathrm{vL}})P_{\mathrm{L}})}}ms + A^2}{\frac{1}{2}C_{\mathrm{vw}}W_{\mathrm{w}}\left|X_{\mathrm{vw}}\right|\sqrt{\frac{1}{\rho(P_{\mathrm{s}} - sgn(X_{\mathrm{vw}})P_{\mathrm{w}})}}ms + A^2} \tag{23}$$

TABLE 1. Rules of fuzzy PID.

$\Delta k_p\vert\ \Delta k_i\vert\ \Delta k_d$		e NB	NS	Z	PS	PB
e_c	NB	PB|NB|PB	PM|NB|PM	PM|NM|PS	PS|NS|Z	Z|Z|Z
	NS	PM|NM|PM	PS|NM|PS	PS|NS|Z	Z|Z|Z	PS|NS|PS
	Z	PM|NM|PM	PS|NS|PS	Z|Z|Z	PS|NS|PS	PM|NM|PM
	PS	PS|NS|PS	Z|Z|Z	PS|NS|Z	PS|NM|PS	PM|NM|PM
	PB	Z|Z|Z	PS|NS|Z	PM|NM|PS	PM|NB|PM	PB|NB|PB

TABLE 2. The information and parameters of key components.

Hydraulic cylinder	Stroke	50 ± 0.5 mm
	Minimum Starting Force	100 N
Servo valve	Nominal Flow	7 L/min
	Natural Frequency	110 Hz
Displacement sensor	Accuracy	0.5%
	Range	60 mm
Force sensor	Accuracy	0.2%
	Range	13000 N
Axial piston pump	Displacement	25 ml/r
	Rated pressure	35 MPa
	Rated speed	2500 r /min

The fuzzy PID controller uses the error e and the error rate e_c as input to meet the requirements of the PID parameters self-tuning by e and e_c at different times. The PID parameters K_p, K_i and K_d are output. The fuzzy control rules are used to modify the PID parameters online so that the fuzzy self-tuning PID controller is constructed [29]. The structure is shown in Fig. 5.

To improve the anti-interference ability of the FCC further, a improved fuzzy PID control is applied. The deviation e of the output force of the FCC and its change rate e_c are defined as the input variables of the fuzzy PID controller, and the three corrections Δk_p, Δk_i, and Δk_d are defined as the output variables. Each domain is defined as follows

The domain of e and e_c $\{-2, -1, 0, 1, 2\}$.

The domain of ΔK_p $\{0, 2, 4, 6\}$.

The domain of ΔK_i $\{-0.3, -0.2, -0.1, 0\}$.

The domain of ΔK_d $\{0, 0.0033, 0.0066, 0.01\}$.

"Positive Big (PB)", "Positive Middle (PM)", "Positive Small (PS)", "Zero (Z)", "Negative Small (NS)", "Negative Middle (NM)" and "Negative Big (NB)" are selected to describe the above variables of the system. The rules of the fuzzy PID are described in TABLE 1.

IV. EXPERIMENTS

A. THE SUPERFLUOUS FORCE UNDER POSITION INTERFERENCE FREQUENCIES

The DCLS includes the hydraulic power system, the detection and control system. The key components information and parameters are described in TABLE 2.

In addition, the detection and control system is constructed by using the personal computer (PC) and the dSPACE controller. The dSPACE controller is used with the Matlab/Simulink software to facilitate communication between the PC control system and the hydraulic system. All control

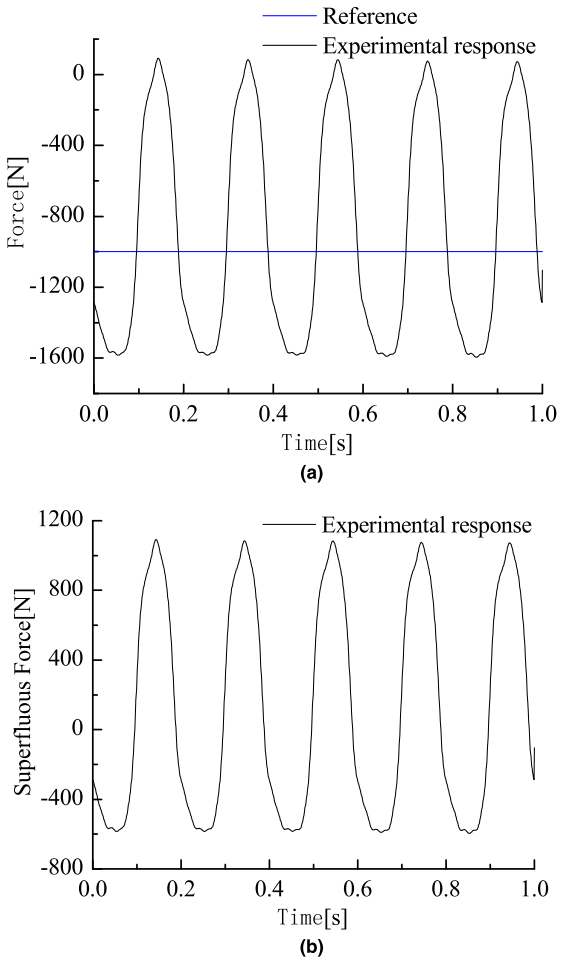

FIGURE 13. Response of FCC at $f_F = 1000$ N. (a) Experimental response curve. (b) Superfluous force curve.

algorithm models are built with Matlab/Simulink. The three former control algorithms are applied by individually and independently opening or closing the "Switch" block.

This experiment uses dSPACE DS1104 control board, which has 8 analog input and output channels, 20 digital input and output channels, and 2 encoder measurements. On the one hand, the control system of MATLAB/Simulink can be compiled by RTI to generate executable code and download it to DS1104PPC controller board to run. On the other hand, the real-time control interface is designed by using the ControlDesk software provided by dSPACE, which realizes the output of the given value of the system control and the collection of experimental data, and monitors the

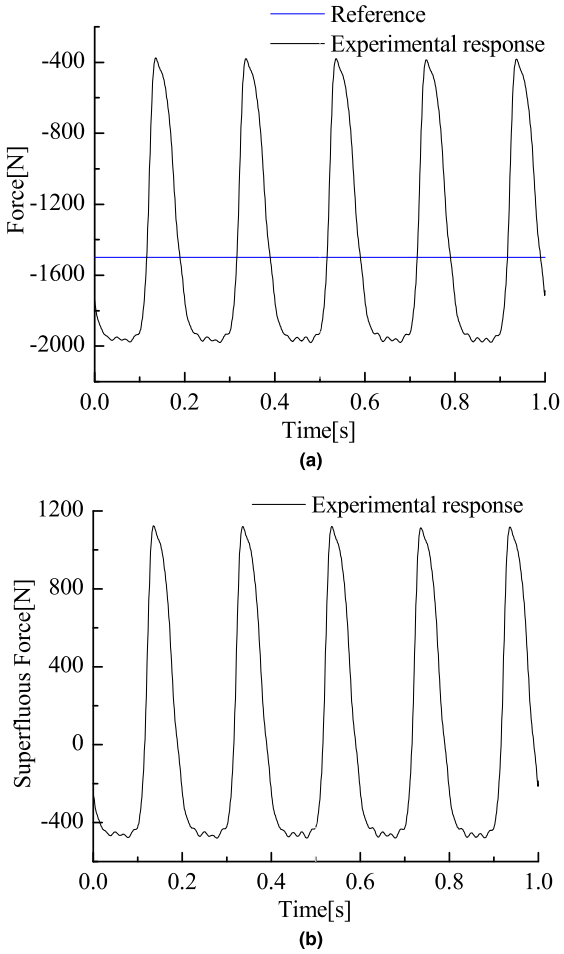

FIGURE 14. Response of FCC at $f_F = 1500$ N. (a) Experimental response curve. (b) Superfluous force curve.

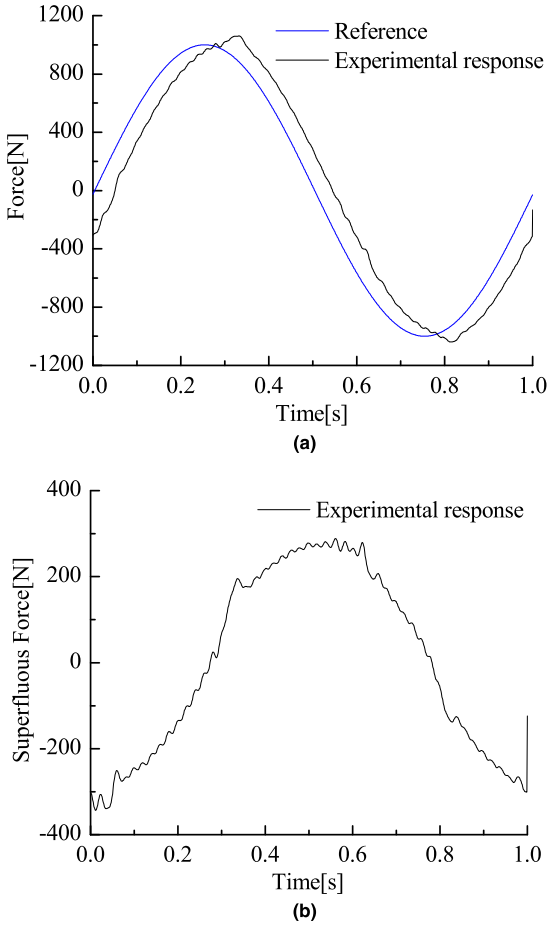

FIGURE 15. Response of FCC at $f_X = 1$ Hz and $f_F = 1$ Hz. (a) Experimental response curve. (b) Superfluous force curve.

whole experimental system in real time to ensure the safe and reliable operation of the system.

During the experiment, the collected acceleration and the pressure signal always contained a high-frequency noise. Therefore, a fourth-order Butterworth digital low-pass filter with a sampling frequency of 1000 Hz and cutoff a frequency of 30 Hz was used to prevent the negative effects caused by noises. The relation between its amplitude and frequency is as follows

$$|H(j\omega)| = \frac{1}{\sqrt{1 + \left(\frac{\omega}{\omega_c}\right)^{2n}}} \tag{24}$$

where n represents the order of the filter, ω_c represents the cut-off frequency of the low pass filter.

The amplitude frequency characteristic curve of the Butterworth low pass filter, which satisfies the performance index, is shown in Fig. 6. From the graph, we can see that the signal within 30 Hz (188.4 rad/s) can pass through completely, and the signal above 30 Hz can be rapidly attenuated, which indicates that the designed Butterworth filter meets the design requirements and has a good filtering performance.

The SSCA, the PSCA and the CCA are applied to restrain the superfluous force during the experiment. When the SSCA and PSCA are used, a normal PID controller is applied in the FCC with $K_P = 6$, $K_I = 3$ and $K_D = 0.01$. When the CCA is used, a fuzzy PID is applied in the FCC with quantization factors $K_e = 2.5$ and $K_{ec} = 0.0025$ and a ratio factor $K_u = 15$.

In the subsequent experiments, the load force is applied to the FCC, and the position interference is applied to the PCC. Their types and values are listed in TABLE 3. To estimate the restraining effects of the different algorithms, we sequentially employ the SSCA, the PSCA, and the CCA.

B. GIVEN SIGNAL AND EXPERIMENTAL RESPONSE

1) STEP GIVEN SIGNAL AND EXPERIMENTAL RESPONSE

At 0.2 s, the loading force of 500 N, 1000 N and 1500 N of FCC is given respectively, and the experimental response curves are shown in Fig. 7.

As can be seen from the above figure, the step response basically has no overshoot. The loading time of 500 N, 1000 N and 1500 N is 0.014 s, 0.024 s and 0.034 s respectively. The DCLS experiment platform can realize step load force loading.

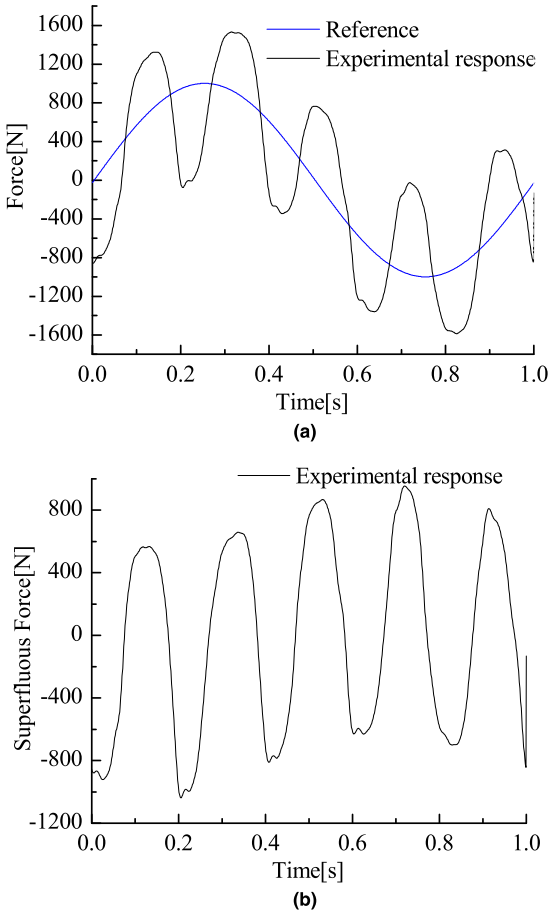

FIGURE 16. Response of FCC at $f_X = 5$ Hz and $f_F = 1$ Hz. (a) Experimental response curve. (b) Superfluous force curve.

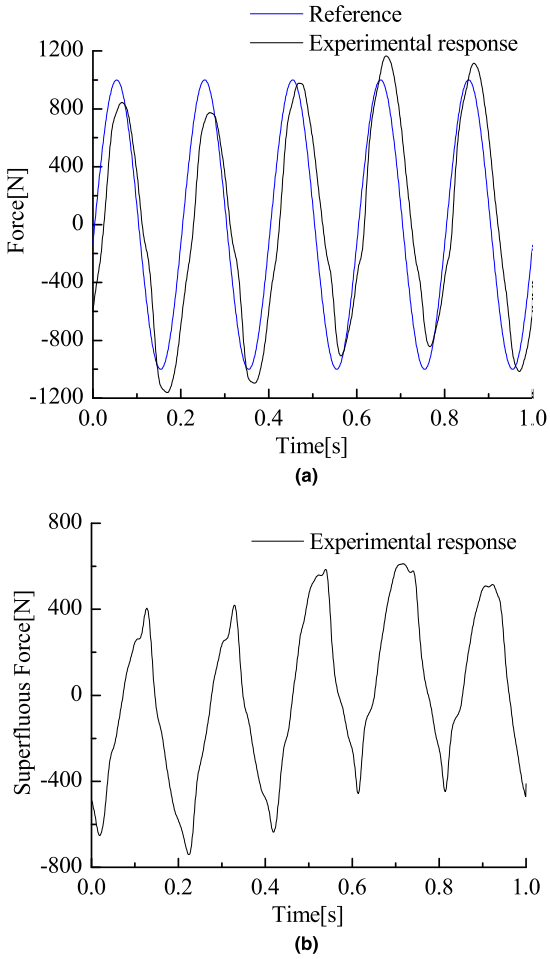

FIGURE 17. Response of FCC at $f_X = 1$ Hz and $f_F = 5$ Hz. (a) Experimental response curve. (b) Superfluous force curve.

2) SINUSOIDAL GIVEN SIGNAL AND EXPERIMENTAL RESPONSE

The sinusoidal force signals with amplitudes of 1000 N and frequencies of 1 Hz, 3 Hz, and 5 Hz are given respectively, and the experimental response curves are shown in Fig. 8.

It is known from the figure that the dynamic tracking precision of FCC is high. When loading to 5 Hz, the amplitude attenuation and the phase angle lag are very small. It shows that the FCC can realize the sinusoidal load of the above frequency better.

The experimental results show that the FCC has a faster response and a higher loading precision in the absence of a position disturbance, which can accurately load the constant load force and the sinusoidal load force. It also shows that the FCC has a good control performance.

C. THE SUPERFLUOUS FORCE

1) EXPERIMENT I

Given the constant value force control signal of FCC 1000 N, the sinusoidal position control signals of PCC with amplitude of 5 mm and frequency of 1 Hz, 3 Hz and 5 Hz are given respectively to carry out experimental research to observe the superfluous force. Fig. 9 to Fig. 11 show the experimental response curves and the superfluous force curves.

2) EXPERIMENT II

Given PCC frequency of 5 Hz, the amplitude of the 5 mm sinusoidal position control signal, respectively, given FCC 0 N, 1000 N, 1500 N constant value force control signal, experimental research to observe the Superfluous force. Fig. 12 to Fig. 14 are the experimental response curves and the superfluous force curves.

3) EXPERIMENT III

A sinusoidal signal with PCC with a frequency of 1 Hz, 5 Hz and an amplitude of 5 mm is given respectively. In addition, a sinusoidal force control signal with FCC with a frequency of 1 Hz, 5 Hz and an amplitude of 1000 N, respectively, is carried out to observe the superfluous force in the experiment. Fig. 15 to Fig. 18 show the experimental response force curves and the superfluous force curves of the FCC.

D. EFFECTS OF RESTRAINING THE SUPERFLUOUS FORCE UNDER POSITION INTERFERENCE FREQUENCIES

First, during **Experiment I,** it could be focused on the influence of the sinusoidal position interference on the superfluous

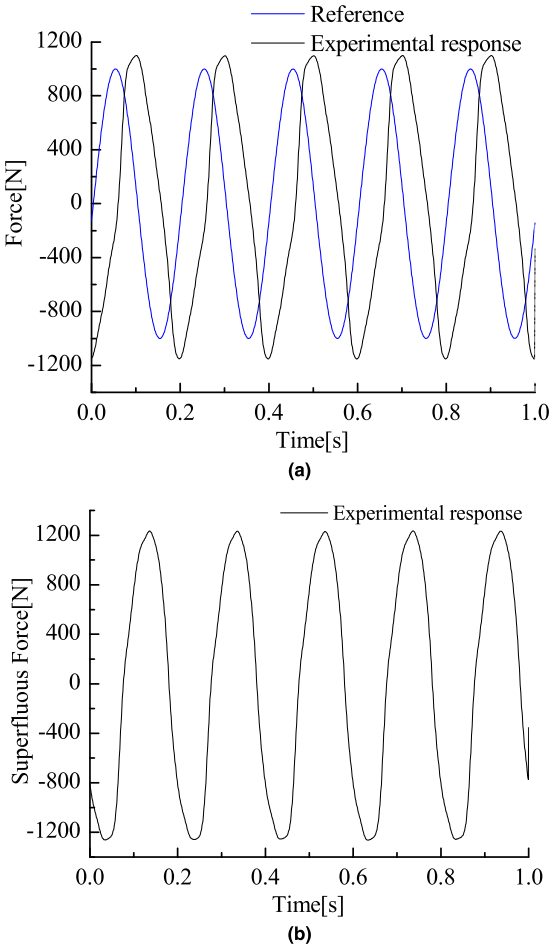

FIGURE 18. Response of FCC at $f_X = 5$ Hz and $f_F = 5$ Hz. (a) Experimental response curve. (b) Superfluous force curve.

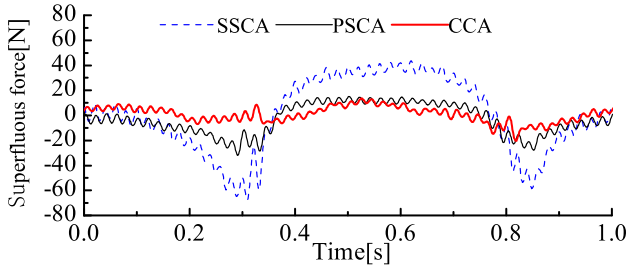

FIGURE 19. Superfluous force curves at $f_X = 1$ Hz.

force. The superfluous force curves for different sinusoidal position interference frequencies are shown in Fig. 19, Fig. 20 and Fig. 21.

To evaluate the effect of the three algorithms, we isolate the peaks of the superfluous forces and describe them with the numerical value shown in TABLE 4.

It indicates that the system lag increases with the increase of position interference frequency by the above curves. The superfluous forces increase while the load accuracies simultaneously decrease. The dynamic nonlinear extent of the compensation link E corresponds with the hydraulic position and may be eliminated largely by the PSCA. For greater

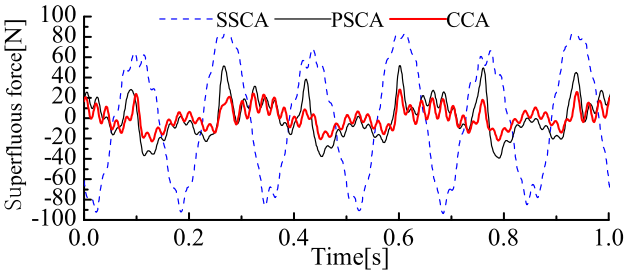

FIGURE 20. Superfluous force curves at $f_X = 3$ Hz.

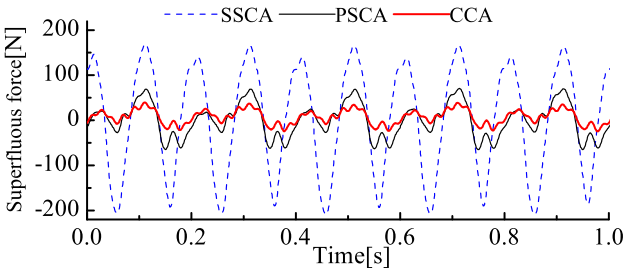

FIGURE 21. Superfluous force curves at $f_X = 5$ Hz.

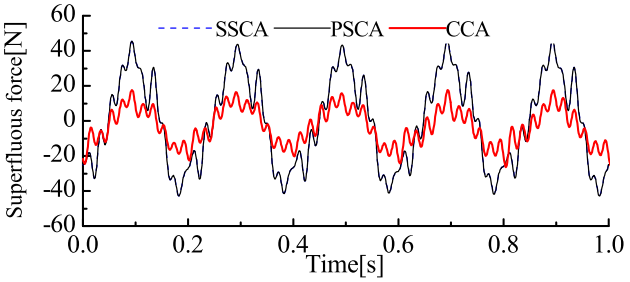

FIGURE 22. Superfluous force curves with $F = 0$ N.

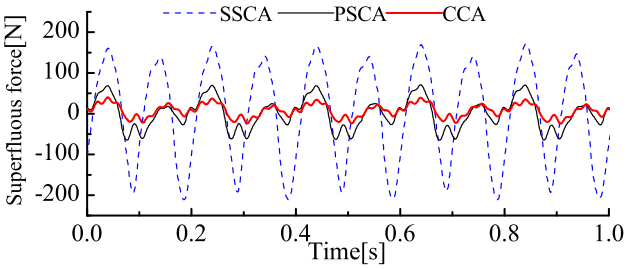

FIGURE 23. Superfluous force curves with $F = 1000$ N.

frequencies, larger percentages may be achieved. Moreover, because the anti-jamming capability of the FCC may be enhanced by the fuzzy PID control, the superfluous force may be suppressed even further when the CCA is applied.

E. EFFECTS OF RESTRAINING THE SUPERFLUOUS FORCE UNDER DIFFERENT LOADING FORCES

Experiment II highlights one addition point regarding the influence of the loading force on the superfluous force.

TABLE 3. The type and values of the force and position exerted in two channels.

Experiment I					
FCC (f_F)			PCC (f_X)		
Signal Type	Value		Signal Type	Amplitude	Frequency
Constant	1000 N		sinusoidal	5 mm	1 Hz, 3 Hz, 5 Hz
Experiment II					
Signal Type	Value		Signal Type	Amplitude	Frequency
Constant	0 N, 1000 N, 1500 N		sinusoidal	5 mm	5 Hz
Experiment III					
Signal Type	Amplitude	Frequency	Signal Type	Amplitude	Frequency
sinusoidal	1000 N	1 Hz, 5 Hz	sinusoidal	5 mm	1 Hz, 5 Hz

TABLE 4. Superfluous forces peak table under different position interference frequency.

Control Method	f_X=1 Hz		f_X=3 Hz		f_X=5 Hz	
	Peak Value	Restrain Effect	Peak Value	Restrain Effect	Peak Value	Restrain Effect
PID	262	0%	647	0%	1091	0%
SSCA	67	74.4%	92	85.8%	180	83.5%
PSCA	32	87.8%	44	93.2%	71	93.5%
CCA	18	93.1%	26	96%	39	96.4%

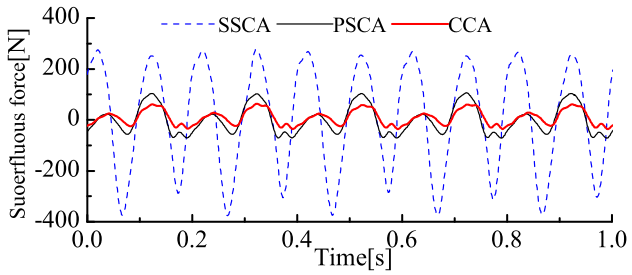

FIGURE 24. Superfluous force curves with $F = 1500$ N.

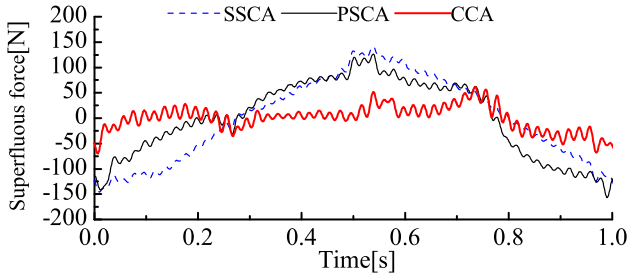

FIGURE 25. Superfluous force curves at $f_X = 1$ Hz and $f_F = 1$ Hz.

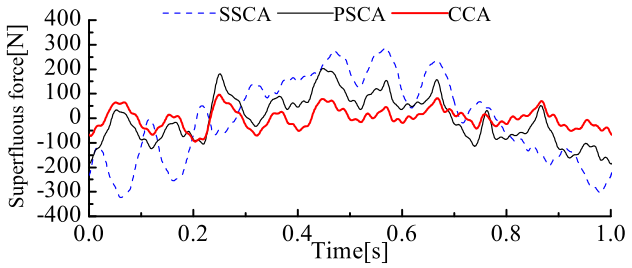

FIGURE 26. Superfluous force curves at $f_X = 5$ Hz and $f_F = 1$ Hz.

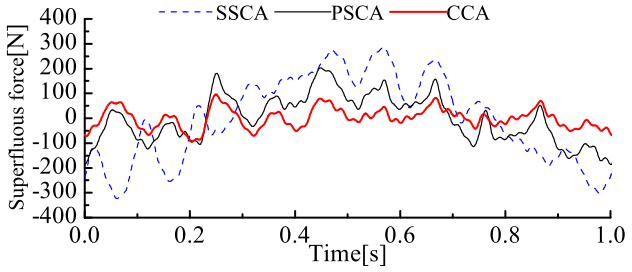

FIGURE 27. Superfluous force curves at $f_X = 1$ Hz and $f_F = 5$ Hz.

The superfluous force curves with different loading forces are shown in Fig. 22, Fig. 23 and Fig. 24.

Moreover, we isolate and describe the peaks of the superfluous forces with the numerical value shown in TABLE 5.

It indicates that the superfluous forces increase while the load accuracies decrease for large loading forces by the above curves. When the FCC is unloaded and the position interference is dynamic, we could obtain the same superfluous force restrained by the PSCA or the SSCA. The dynamic nonlinear extent of the compensation link E has little correspondence with the hydraulic force and may be largely eliminated by the PSCA. Obviously, when the loading force is 1000 N and 1500 N, the PSCA is more suitable for the loading system. Moreover, if fuzzy PID control is employed, the loading force could adaptively be tuned online. Therefore, the superfluous forces are further decreased. This illustrates that we really could obtain better restraining effect for the FCC if the CCA is employed.

TABLE 5. Superfluous forces peak table under different force loads.

Control Method	f_F =0 N		f_F =1000 N		f_F =1500 N	
	Peak Value	Restrain Effect	Peak Value	Restrain Effect	Peak Value	Restrain Effect
PID	872	0%	1091	0%	1123	0%
SSCA	45	94.8%	180	83.5%	278	75.2%
PSCA	45	94.8%	71	93.5%	106	90.6%
CCA	22	97.5%	39	96.4%	65	94.2%

TABLE 6. Table of the superfluous force peaks with sinusoidal interference in the position and the loading force.

Control Method	f_X=1 Hz f_F=1 Hz		f_X=5 Hz f_F=1 Hz		f_X=1 Hz f_F=5 Hz		f_X=5 Hz f_F=5 Hz	
	Peak Value	Restrain Effect	Peak Value	Restrain Effect	Peak Value	Restrain Effect	Peak Value	Restrain Effect
PID	343	0%	1038	0%	651	0%	1204	0%
SSCA	155	54.8%	322	69.0%	570	12.4%	625	48.1%
PSCA	140	59.2%	203	80.4%	384	41.0%	411	65.9%
CCA	63	81.6%	95	90.8%	211	67.6%	209	82.6%

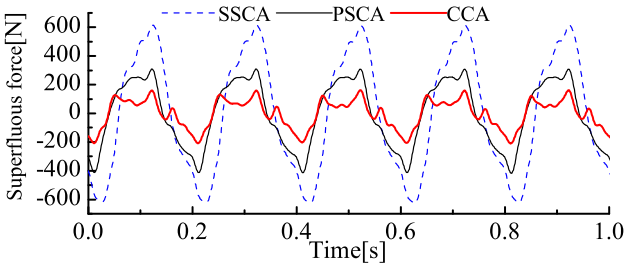

FIGURE 28. Superfluous force curves at $f_X = 5$ Hz and $f_F = 5$ Hz.

F. EFFECTS OF RESTRAINING THE SUPERFLUOUS FORCE WITH SINUSOIDAL INTERFERENCE IN THE POSITION AND THE LOADING FORCE

Experiment III focuses on the influence of the loading force and the position interference on the superfluous force. Therefore, for this section, there are four series of experiments should be carried out. The initial sinusoidal phases of the loading force and the position interference are similar. The superfluous force curves are shown in Fig. 25, Fig. 26, Fig. 27and Fig. 28. Similarly, we isolate and describe the superfluous force peaks with the numerical value shown in TABLE 6.

The above curves indicate that for the same reason, although the loading forces are dynamic, the restraining control algorithms are all effective. The superfluous forces successively decrease for the SSCA, the PSCA and the CCA. In particular, the superfluous force restrained by the CCA is reduced to 81.6%, 90.8%, 67.6% and 82.6%. This shows that the CCA is more suitable for restraining the superfluous force under dynamic loads.

V. CONCLUSION

The DCLS was conducted to assess the performance of the HDU which is used for the HQR. The mathematical model of the position disturbance and the loading force of the HDU were developed using the mechanism modeling method. To fulfill the stringent high performance requirement of the HDU, the three control algorithms (i.e., the SSCA, the PSCA and the CCA) are researched to restrain the nonlinear superfluous force.

SSCA can restrain superfluous force to a large extent. The higher the position disturbance frequency is, the more obvious the restraint effect is. When no load is applied, the superfluous force is almost completely eliminated. With the increase of the load force, SSCA restraining the superfluous force is getting worse. When the load frequency is high, the restraint effect is not good. SSCA is not effective in dynamic loading.

While it is helpful to use the SSCA for restraining the superfluous force, the pressure-flow nonlinearity of the servovalve cannot be overcome. The PSCA was designed by the same principle as the SSCA, but its compensation link E can adaptively compensate for the dynamic nonlinearities online. Therefore, we could obtain better restraining effect. When the load force is larger, the restraint effect of PSCA become better. Applying PSCA, the accuracy of load dynamic tracking needs to be further improved. It is particularly suitable for a system with high-frequency interference and a substantial loading force.

Since the anti-jamming capability of the FCC is improved by fuzzy PID control, the CCA better weakens the position interference. It further restrains the superfluous force, and it is more suitable for a dynamic loading force system.

Furthermore, the frequency of the dynamic loading force and the position interference are small. We are not sure whether the three control algorithms are effective for practical applications of the HRQ or not. Therefore, some experiments should be designed for practical applications when the HQR is loaded into the DCLS.

REFERENCES

[1] T. Chen, X.-W. Rong, Y.-B. Li, C. Ding, H. Chai, and L.-L. Zhou, "A compliant control method for robust trot motion of hydraulic actuated quadruped robot," *Int. J. Adv. Robot. Syst.*, vol. 15, no. 6, pp. 1–16, Oct. 2018.

[2] T. Boaventura, G. A. Medrano-Cerda, C. Semini, J. Buchli, and D. G. Caldwell, "Stability and performance of the compliance controller of the quadruped robot HyQ," in *Proc. IEEE/RSJ Int. Conf. Intell. Robots Syst.*, Nov. 2013, pp. 1458–1464.

[3] T. Boaventura, J. Buchli, C. Semini, and D. G. Caldwell, "Model-based hydraulic impedance control for dynamic robots," *IEEE Trans. Robot.*, vol. 31, no. 6, pp. 1324–1336, Dec. 2015.

[4] V. H. Duy, "Control of the quadruped robot using simple CPG network," in *Proc. 7th IEEE Conf. Ind. Electron. Appl. (ICIEA)*, Jul. 2012, pp. 512–517.

[5] Z.-C. Pei, L. Song, B. Chen, and X.-Q. Guo, "Adaptive control of a quadruped robot based on central pattern generators," in *Proc. 10th Int. Conf. Ind. Inform.*, Jul. 2012, pp. 554–558.

[6] S. A. A. Moosavian, M. Khorram, A. Zamani, and H. Abedini, "PD regulated sliding mode control of a quadruped robot," in *Proc. IEEE Int. Conf. Mechatronics Automat.*, Aug. 2011, pp. 2061–2066.

[7] C.-Y. Luo, J.-Y. Yao, F.-H. Chen, L. Li, and Q. Xu, "Adaptive repetitive control of hydraulic load simulator with RISE feedback," *IEEE Access*, vol. 5, pp. 23901–23911, 2017.

[8] Q. Feng, G. Xiaoqiang, Y. Bo, and P. Zhongcai, "Theoretical analysis of surplus torque in electro-hydraulic load simulator," in *Proc. Int. Conf. Fluid Power Mechatronics*, Aug. 2011, pp. 150–153.

[9] G.-Q. Li, H.-Y. Yang, S.-C. Li, and Y. Zhao, "Research on decoupling control for electro-hydraulic load simulator," in *Proc. Int. Conf. Adv. Mechtron. Syst.*, Sep. 2012, pp. 473–477.

[10] J.-Y. Li, J.-P. Shao, Z.-W. WangBo, and W. Guihua Han, "Study of the electro-hydraulic load simulator based on double servo valve concurrent control," in *Proc. 9th Int. Conf. Electron. Meas. Instrum.*, Aug. 2009, pp. 30–33.

[11] J.-Y. Li, J.-P. Shao, G.-H. Han, Z.-W. Wang, and B. Wu, "Study of the electro-hydraulic load simulator based on flow-press servo valve and flow servo valve parallel control," in *Proc. Int. Conf. Intell. Hum.-Mach. Syst. Cybern.*, Hangzhou, China, Aug. 2009, pp. 70–74.

[12] D. Q. Truong and K. K. Ahn, "Parallel control for electro-hydraulic load simulator using online self tuning fuzzy PID technique," *Asian J. Control*, vol. 13, no. 4, pp. 522–541, 2011.

[13] Y.-L. Fu, Y. Pang, H. Liu, and Y. Zhang, "Force fighting research of dual redundant hydraulic actuation system," in *Proc. Int. Conf. Intell. Syst. Design Eng. Appl.*, Oct. 2010, pp. 762–766.

[14] G.-J. Liu, Y.-H. Li, and L.-M. Yang, "Accurate mathematical model for describing electrohydraulic loading system of helicopter pitch adjusting hydromechanical servos," in *Proc. Conf. Robot., Automat. Mechatronics*, Jun. 2010, pp. 309–314.

[15] G.-Q. Li, J. Cao, B. Zhang, and K.-D. Zhao, "Design of robust controller in electrohydraulic load simulator," in *Proc. Int. Conf. Mach. Learn. Cybern.*, Dalian, China, Aug. 2006, pp. 779–784.

[16] N. Niksefat and N. Sepehri, "Designing robust force control of hydraulic actuators despite system and environmental uncertainties," *IEEE Control Syst.*, vol. 21, no. 2, pp. 66–77, Apr. 2001.

[17] K. K. Ahn and Q. T. Dinh, "Self-tuning of quantitative feedback theory for force control of an electro-hydraulic test machine," *Control Eng. Pract.*, vol. 17, no. 11, pp. 1291–1306, 2009.

[18] D. Zheng and H.-G. Xu, "Robust H∞control of a friction based electrohydraulic load simulator," in *Proc. 29th Chin. Control Decis. Conf. (CCDC)*, May 2017, pp. 3961–3966.

[19] R.-B. Yuan, K.-D. Zhao, and G.-Q. Li, "Control of load simulator based on mixed sensitivity method," *J. Nanjing Univ. Sci. Technol.*, vol. 30, no. 5, p. 537, Oct. 2006.

[20] P. Skupin, W. Klopot, and T. Klopot, "Dynamic Matrix Control with Partial Decoupling," in *Proc. 11th WSEAS Int. Conf. Automat. Inf.*, Jun. 2010, pp. 61–66.

[21] H. Wang, Y.-Y. Gao, and Y.-S. Shi, "Research on controller design and simulation of electro-hydraulic servo system," in *Proc. Int. Conf. Mechatronics Automat.*, Aug. 2010, pp. 35–38.

[22] K. K. Ahn, D. Q. Truong, and T. Q. Thanh, "Online self-tuning fuzzy proportional–integral–derivative control for hydraulic load simulator," *J. Syst. Control Eng.*, vol. 222, no. 2, pp. 81–95, 2008.

[23] D. Q. Truong and K. K. Ahn, "Force control for hydraulic load simulator using self-tuning grey predictor—Fuzzy PID," *Mechatronics*, vol. 19, no. 2, pp. 233–246, Mar. 2009.

[24] Z.-X. Jiao, J. X. Gao, H. Qing, and S. P. Wang, "The velocity synchronizing control on the electro-hydraulic load simulator," *Chin. J. Aeronaut.*, vol. 17, no. 1, pp. 39–46, 2004.

[25] C.-W. Wang, Z.-X. Jiao, and C.-J. Luo, "An improved velocity synchronization control on electro-hydraulic load simulator," *Acta Aeronaut. Astronaut. Sinica*, vol. 33, no. 9, pp. 84–92, 2012.

[26] G. Jacazio and L. Gastaldi, "Equalization techniques for dual redundant electro hydraulic servo actuators for flight control systems," in *Proc. Bath/ASME Symp. Fluid Power Motion Control*, Oct. 2008, pp. 543–557.

[27] G.-Z. Zhou, D. Guo, and X.-Y. Qi, "A superfluous force suppression method based on structure invariance principle with particle swarm optimization algorithm," *Adv. Mater. Res.*, vol. 430, pp. 1877–1880, Jan. 2012.

[28] L.-P. Zhang, *The Hydraulic Control System and Design*. Beijing, China: Chemical Industry Press, 2007, pp. 239–253.

[29] S.-Y. Wang, Y. Shi, and Z.-X. Feng, "A method for controlling a loading system based on a fuzzy PID controller," *Mech. Sci. Technol. Aerosp. Eng.*, vol. 30, no. 1, p. 30, Jan. 2011.

LINGXIAO QUAN was born in Weinan, Shanxi, China, in 1977. He received the B.S., M.S., and Ph.D. degrees in mechanical engineering from Yanshan University, Qinhuangdao, China, in 2000, 2005, and 2010, respectively.

From 2010 to 2013, he was a Lecturer with the Mechanical Engineering Department, Yanshan University, where he is currently an Associate Professor. He has authored more than 54 academic papers. He held 26 patents. His main research fields include mechanism design and control technology of high-end rehabilitation medical robot, vibration mechanism and control technology of aerospace hydraulic components and systems, and the design and development of high-performance electro-hydraulic servo control systems. The main awards include the Hebei Science and Technology Award, the China Industry-University-Research Cooperation Innovation Achievement Award, and the Shanghai Science and Technology Award.

YAOYAO MIAO was born in Handan, China, in 1992. He received the B.S. degree in mechanical engineering from Yanshan University, Qinhuangdao, China, in 2015, where he is currently pursuing the M.S. degree.

His research interest includes vibration mechanism and the control technology of aerospace hydraulic components and systems.

CHANGHONG GUO was born in Qinhuangdao, Hebei, China, in 1977. She received the B.S. degree in the process and equipment of machinery manufacturing from Yanshan University, in 1999, and the M.S. degree in aerospace engineering from the Beijing University of Aeronautics and Astronautics, in 2004.

From 2015 to 2016, she was a Guest Researcher with the Institute of Precision and Automation Control of Agricultural Machinery, Washington State University. Since 2013, she has been an Associate Professor with the Mechanical Engineering Department, Yanshan University. Her main research interests include mechanical design, aerospace manufacturing engineering, and materials science.

QIN ZHANG received the B.S. degree in mechanical engineering from Zhejiang Agricultural University, Zhejiang, China, in 1982, the M.S. degree in agricultural engineering from the University of Idaho, in 1988, and the Ph.D. degree in agricultural engineering from the University of Illinois at Urbana–Champaign, in 1991.

Since 2009, he has been a Professor with Washington State University. He has authored three books and more than 114 academic papers. He holds 10 U.S. patents. He is primarily interested in agricultural machinery automation (automated and autonomous agricultural machinery technologies, and intelligent agricultural machinery controls), and agriculture automation (on-machinery crop health sensing technologies, machinery-area network technologies, and agricultural infotronics technologies).